

Impact of Ly α heating on the global 21-cm signal from the Cosmic Dawn

Raghunath Ghara^{1*}, Garrelt Mellema¹

¹ Department of Astronomy & Oskar Klein Centre, AlbaNova, Stockholm University, SE-106 91 Stockholm, Sweden

Accepted XXX. Received YYY; in original form ZZZ

ABSTRACT

The resonance scattering of Ly α photons with neutral hydrogen atoms in the IGM not only couples the spin temperature to the kinetic temperature but also leads to a heating of the gas. We investigate the impact of this heating on the average brightness temperature of the 21-cm signal from the Cosmic Dawn in the context of the claimed detection by the EDGES low-band experiment. We model the evolution of the global signal taking into account the Ly α coupling and heating and a cooling which can be stronger than the Hubble cooling. Using the claimed detection at $z \approx 17$ from the EDGES low-band observations as a constraint, we find that a strong Ly α background is ruled out. Instead the results favour a weak Ly α background combined with an excess cooling mechanism which is substantially stronger than previously considered.

Key words: galaxies: formation - intergalactic medium - cosmology: theory - dark ages, reionization, first stars

1 INTRODUCTION

The formation of the first sources of light is one of the milestone events in the history of our Universe. These primordial sources changed the ionization and thermal state of the gas in the intergalactic medium (IGM) and thus affected the further evolution of the Universe. The period when these very first sources formed is sometimes called the ‘Cosmic Dawn’ (CD). Details regarding these early sources, such as the time of their formation, their emission properties, etc. remain unknown. Models such as in Furlanetto & Pritchard (2006); Mesinger et al. (2013); Fialkov et al. (2017); Cohen et al. (2018); Park et al. (2019); Mirocha & Furlanetto (2019), suggest that the first sources formed around redshift 30 and their ultraviolet radiation first caused the spin temperature of the neutral hydrogen in the IGM to change due to repetitive scattering of Lyman series photons, a process known as the Wouthuysen-Field effect (Wouthuysen 1952; Field 1958; Hirata 2006). The same models also predict that over time X-rays produced by these sources started to heat the IGM and only much later, in what usually is called the Epoch of Reionization (EoR) sufficient numbers of ionizing photons were produced to reionize the Universe.

The 21-cm signal produced by the neutral hydrogen in the IGM during these epochs can provide us with answers to many of the questions regarding the CD and the EoR. Therefore several efforts to detect this signal have been initiated. Two different types of experiments exist. The first kind uses large interferometers to measure the spatial fluctuations of the neutral hydrogen (H I) signal in terms of statistical quantities such as the power spectrum.

Examples of these are the Low Frequency Array (LOFAR)¹ (van Haarlem et al. 2013; Patil et al. 2017), the Giant Metrewave Radio Telescope (GMRT)² (Ghosh et al. 2012; Paciga et al. 2013), the Precision Array for Probing the Epoch of Reionization (PAPER)³ (Parsons et al. 2014) and the Murchison Widefield Array (MWA)⁴ (Bowman et al. 2013; Tingay et al. 2013). The future low frequency component of the Square Kilometre Array (SKA-Low)⁵ will have the sensitivity to directly probe the spatial structure of the fluctuations by producing images of the signal (Mellema et al. 2015; Ghara et al. 2016). The second type of experiment tries to detect the sky-averaged 21-cm signal, a quantity which the interferometers are unable to measure. Such a measurement only requires a single antenna. Examples of this type are EDGES (Bowman & Rogers 2010), SARAS (Patra et al. 2015), BigHorns (Sokolowski et al. 2015), SciHi (Voytek et al. 2014) and LEDA (Greenhill & Bernardi 2012).

However, the detection of the redshifted 21-cm signal from the EoR and CD is very challenging for all types of experiments as it is several orders of magnitude weaker than the galactic and extra-galactic foreground signals at these frequencies. In addition, long integration times are needed to bring the system noise below the cosmological signal which makes calibration challenging, not only because of instrument stability but also because of the impact

¹ <http://www.lofar.org/>

² <http://www.gmrt.tifr.res.in>

³ <http://eor.berkeley.edu/>

⁴ <http://www.mwatelescope.org/>

⁵ <http://www.skatelescope.org/>

* E-mail: ghara.raghunath@gmail.com

of time-dependent ionospheric effects. As a consequence, no undisputed detections of the signal have yet been made.

The strength of the redshifted 21-cm signal from the CD depends on the gas temperature and background Ly α flux which are determined by the radiation sources and the heating/cooling processes. Several heating processes such as X-ray heating (Pritchard & Furlanetto 2007; Mesinger et al. 2013; Ghara et al. 2015; Ross et al. 2018), shock heating (Furlanetto & Loeb 2004) and heating due to resonance scattering of Ly α photons (hereafter ‘Ly α heating’) (Chen & Miralda-Escudé 2004; Chuzhoy & Shapiro 2007; Furlanetto & Pritchard 2006) can increase the kinetic temperature of the gas in the IGM during these epochs. However, the relative contribution of these mechanisms is uncertain. In addition to these heating processes based on known physics, unknown physics such as dark matter decay may also convey energy to the IGM (Clark et al. 2018; Mitridate & Podo 2018; Liu & Slatyer 2018a). The gas cooling is expected to be dominated by the adiabatic cooling due to the expansion of the Universe (‘Hubble cooling’) with radiative cooling due to e.g. recombinations playing a subdominant role.

Recently, Bowman et al. (2018) claimed a detection of a redshift-amplitude profile of the global 21-cm signal around redshift $z \sim 17$ from observations with the EDGES low-band instrument. However, the measured signal is stronger by several factors than the signal predicted by the previous theoretical studies such as Pritchard & Furlanetto (2007); Mesinger et al. (2013); Santos et al. (2008); Ghara et al. (2015). Explanations for the EDGES low-band results fall into two categories. The first kind assumes a lower than expected IGM temperature due to excess cooling caused by an unknown physical process such as the interaction between baryons and dark matter particles (Barkana 2018; Fialkov et al. 2018; Muñoz & Loeb 2018; Berlin et al. 2018). The second type considers an excess radio background which can also enhance the measurement of the H I signal, which is otherwise seen against the background of the Cosmic Microwave Background (CMB) (Feng & Holder 2018; Ewall-Wice et al. 2018; Fraser et al. 2018). However, the excess radio background required to explain EDGES low-band results is unlikely as the time scale for generating a radio background is several order of magnitude shorter than the duration of the EDGES signal centred at redshift ~ 17 (Sharma 2018). In addition, the required excess radiation background to explain EDGES result needs $\sim 10^3$ times larger emission of 1-2 GHz photons than observed at local galaxies (Mirocha & Furlanetto 2019).

Both of these explanations require the spin temperature to be strongly coupled to the gas temperature which requires a strong Ly α background. However, these Ly α photons will also heat up the gas by resonance scattering. The question is whether this heating effect has an impact on the global signal. Madau et al. (1997) estimated the heating rate due to resonance scattering assuming that the scattering occur with atoms at rest. For this estimate, the IGM temperature would exceed the CMB temperature in a fraction of Hubble time. A subsequent paper by Chen & Miralda-Escudé (2004) included the effect of atomic thermal motions into the calculation and showed that the Ly α heating rate is at least three orders of magnitude lower than estimated in Madau et al. (1997). Their calculation considered heating due to photons between Ly α and Ly β (so-called ‘continuum photons’) as these redshifts into Ly α resonance and cooling due to the cascade of higher resonance states into Ly α (so-called ‘injected photons’). These authors showed that these two mechanism balance at a temperature ~ 10 K and thus the temperature would not increase beyond that. This low equilibrium value has prompted many works to neglect Ly α heating as its effect would seem to be negligible compared to for example X-ray

heating. However, both these works did not consider the forbidden transition from the 2s to the 1s level of hydrogen, something which was added to the calculation by Chuzhoy & Shapiro (2007) who furthermore included the effect of deuterium. The result is a lower cooling contribution from the injected photons and which implies that the gas temperature can increase to an equilibrium value of ~ 100 K prior to the reionization.

Previous studies of the global 21-cm signal in the context of the EDGES results did either not consider Ly α heating (see e.g., D’Amico et al. 2018; Liu & Slatyer 2018b; Schneider 2018; Barkana et al. 2018; Nebrin et al. 2018) or used the erroneously low values from Chen & Miralda-Escudé (2004) (see e.g., Fialkov & Barkana 2019; Venumadhav et al. 2018). In this study, we for the first time adopt the calculation of the Ly α heating rates from Chuzhoy & Shapiro (2007) and investigate its impact on the global 21-cm signal from the CD. We include excess cooling so as to be able to reproduce EDGES low-band observations. We explore the parameter space of Ly α heating and excess cooling to study the absorption profile of the global signal to find combinations of parameters that agree with the EDGES low-band results.

We have organised the paper in the following way. In section 2 we describe the analytical model we use to calculate the evolution of the global 21-cm signal, including the heating rates due to resonance scattering of the Ly α photons and the excess cooling needed to explain the EDGES result. We present our results in section 3 before we conclude in section 4. We use the cosmological parameters $\Omega_m = 0.32$, $\Omega_B = 0.049$, $\Omega_\Lambda = 0.68$, $h = 0.67$, $\sigma_8 = 0.83$ and $n_s = 0.96$ throughout the paper (Planck Collaboration et al. 2016).

2 MODEL FOR 21-CM SIGNAL

2.1 Analytical model

The 21-cm signal from the H I gas is measured as the differential brightness temperature against the CMB and can be written as

$$\delta T_b = 27 x_{\text{HI}}(1+\delta_B) \left(\frac{\Omega_B h^2}{0.023} \right) \sqrt{\frac{0.15}{\Omega_m h^2} \frac{1+z}{10}} \left(1 - \frac{T_\gamma}{T_S} \right) \text{ mK}, \quad (1)$$

where x_{HI} , δ_B , T_S and $T_\gamma = 2.73 \times (1+z)$ K denote the neutral fraction, density contrast, the spin temperature of the hydrogen gas and the CMB temperature at redshift z respectively. Here, we adopt an analytic approach as described below to model the expected 21-cm signal in presence of spin temperature fluctuations.

The analytical model follows previous works such as Pritchard & Furlanetto (2007); McQuinn et al. (2005). It incorporates Ly α , UV and X-ray photons from the sources which are taken to be associated with dark matter halos. The number of dark matter halos at a given redshift is determined using the Press-Schechter halo mass function assuming that only halos with Virial temperatures above 10^4 K contribute.

It estimates the volume averaged ionization fractions of the highly ionized H II regions (x_i) and largely neutral gas in the IGM outside these H II regions (x_e). We assume the temperature of the ionized H II regions to be $\sim 10^4$ K. The code estimates the gas temperature (T_K) of the largely neutral medium outside the H II regions following the heating and cooling processes.

The heating rate due to resonance scattering as well as the spin temperature coupling depends crucially on the number of Ly α photons emitted from the sources. Here we follow Furlanetto & Pritchard (2006) to estimate the average Ly α photon flux. We assume a power law spectrum $\epsilon_s(\nu) = f_\alpha A_\alpha \nu^{-\alpha_s - 1}$ between Ly α

and Ly β and between Ly β and the Lyman limit, where the power law indices α_s can differ. The spectral index α_s between Ly α and Ly β is taken to be 0.14 which corresponds to population II type sources. The normalization factor A_α is estimated such that the number of Ly α photons per baryon in the range Ly α -Ly β is 6520 for $f_\alpha = 1$. The spectral index in the range Ly α -Lyman limit is adjusted so that the total number of photons per baryon for this wavelength regime is 9690. The parameter f_α determines the production rate of the Ly α photons from the stars. The heating rate due to Ly α scattering is described below in Section 2.2.

For the X-ray heating, we follow Pritchard & Furlanetto (2007) and assume that the emissivity of X-ray photons from the sources follows the star formation rate density. We use an X-ray spectral distribution given by

$$\epsilon_X(\nu) = \frac{L_0}{h\nu_0} \left(\frac{\nu}{\nu_0} \right)^{-\alpha_X - 1} \quad (2)$$

with $L_0 = f_X \times 10^{41} \text{ erg s}^{-1} \text{ Mpc}^{-3}$, $h\nu_0 = 1 \text{ keV}$. We choose X-ray efficiency parameter $f_X = 1$ and the spectral index of the X-ray spectrum $\alpha_X = 0.5$ for the fiducial X-ray source. Note that for most of our results we will set $f_X = 0$ as the fiducial X-ray source model will be used only to compare Ly α and X-ray heating.

Finally our model also includes the effect of ionizing UV radiation. The rate of emission of the UV photons per baryon is

$$\Lambda_i = \zeta \frac{df_{\text{coll}}}{dt}. \quad (3)$$

The ionization efficiency parameter $\zeta = N_{\text{ion}} \times f_{\text{esc}} \times f_\star$ depends on the average number of ionizing photons per baryon produced in the stars (N_{ion}), the star formation efficiency (f_\star) and the escape fraction of the UV photons (f_{esc}). All these quantities are uncertain during the CD and EoR. In this study, we assume $N_{\text{ion}} = 4000$ which corresponds to population II types of stars, $f_\star = 0.1$ and $f_{\text{esc}} = 0.1$ for modelling reionization. We note however that for most of our results ionization levels remain very low and do not impact the global 21-cm signal.

2.2 Heating due to resonance scattering

To estimate the heating rates due to the resonance scattering, we follow the calculations of Chuzhoy & Shapiro (2007). Photons emitted with frequencies between Ly α and Ly β frequency (‘continuum photons’) will redshift to the Ly α frequency at which point they suffer resonance scattering by H I. This process will heat up the gas. On the other hand, photons with a wavelength between Ly β and Lyman limit will be absorbed by the hydrogen atoms after redshifting to Ly β or other higher Lyman series lines. If higher resonance or excited states first decay to $2p$ state and then to the ground state, one Ly α photon will be emitted. In contrast to the continuum photons, the emission of the Ly α photons (‘injected photons’) due to the cascade of from the higher levels will cool the gas. The spectrum gets affected once the photons redshift through the Ly α resonance. The intensity $J(\nu)$ at a frequency ν in the vicinity of the resonance frequency ν_α can be written as (Chuzhoy & Shapiro 2007),

$$J(x) = J(0)e^{-\frac{2\pi\gamma x^3}{3a} - 2\eta x}, \quad (4)$$

for the injected photons. The above expression also hold for the continuum photons with $x > 0$, otherwise

$$J(x) = 2\pi J_0 \gamma a^{-1} \int_{-\infty}^x e^{\frac{2\pi\gamma(z^3 - x^3)}{3a} + 2\eta(z - x)} dz. \quad (5)$$

where

$$\begin{aligned} x &= (\nu/\nu_\alpha - 1)/(2k_B T_K/mc^2)^{1/2}, \\ a &= A_{21}(2k_B T_K/mc^2)^{-1/2}/4\pi\nu_\alpha, \\ \gamma &= \tau_{\text{GP}}^{-1}(1 + 0.4/T_S)^{-1}, \end{aligned} \quad (6)$$

$$\eta = [h\nu_\alpha/(2k_B T_K mc^2)^{1/2}][(1 + 0.4/T_S)/(1 + 0.4/T_K)].$$

Here k_B , m , c and A_{21} are the Boltzmann constant, mass of hydrogen atom, speed of light and the Einstein spontaneous emission coefficient of Ly α transition respectively. The quantities τ_{GP} and J_0 are the Gunn-Peterson optical depth and the UV intensity at a frequency far away from ν_α respectively.

Here $J(0)$ can be expressed as,

$$\frac{J(0)}{J_0} = \frac{\pi\zeta (J_{1/3}(\zeta) - J_{-1/3}(\zeta))}{\sqrt{3}} + {}_1F_2(1; 1/3, 2/3, -\zeta^2/4) \quad (7)$$

where $\zeta = \sqrt{16\eta^3 a/9\pi\gamma}$, ${}_1F_2$ is hyper-geometric function, $J_{1/3}$ and $J_{-1/3}$ are the Bessel functions of first kind respectively.

The total heating/cooling rate due to the resonance scattering can be written as,

$$\frac{d \log T_K}{d \log t} \Big|_{\text{heating}} = \frac{2t}{3k_B T_K} H_\alpha, \quad (8)$$

where t represents time, H_α is the rate of exchange of total energy by the photons due to resonance scattering.

$$H_\alpha = \dot{N}_\alpha \left(\Delta E_c + \frac{J_i}{J_c} \Delta E_i \right) \quad (9)$$

where \dot{N}_α denotes the number of photons per hydrogen atom that pass through resonance scattering per unit time. The ratio of injected and continuum photons J_i/J_c depends on the source’s surface temperature. We choose $J_i/J_c \approx 0.1$ which corresponds to a source with an effective temperature $\lesssim 5 \times 10^4 \text{ K}$ which corresponds approximately to population II type of sources (Chuzhoy & Shapiro 2007). The quantities ΔE_c and ΔE_i are the total energy gain by the gas due to a resonance scattering by the continuum and injected photons respectively. This can be written as,

$$\Delta E(x) = \frac{(h\nu)^2}{mc^2} \int \frac{J(x)}{J_0} \phi(x) dx \quad (10)$$

where $\phi(x)$ is the normalized scattering cross-section. Note that Chuzhoy & Shapiro (2007) also considered the heating contribution from deuterium in their studies. Here we have not included this and thus our calculations somewhat underestimate the actual heating rates.

2.3 Cooling processes

The gas temperature of the IGM is one of the key quantities which determine the strength and nature of the 21-cm signal from the CD. As the heating and cooling processes during those epochs are uncertain, the gas temperature as well as the signal are also poorly understood. The analytical method used in this study incorporates the adiabatic cooling due to the expansion of the Universe which dominates over radiative processes such as the collisional-ionization cooling, recombination cooling, collisional excitation cooling, free-free cooling, etc. After Compton scattering with CMB photons ceases to be important, this Hubble cooling causes the average gas temperature to evolve as $T_K \propto (1+z)^2$. For standard physics, the post-recombination gas temperature is easily calculated, as can for example be done with the publicly available code RECFast (Seager

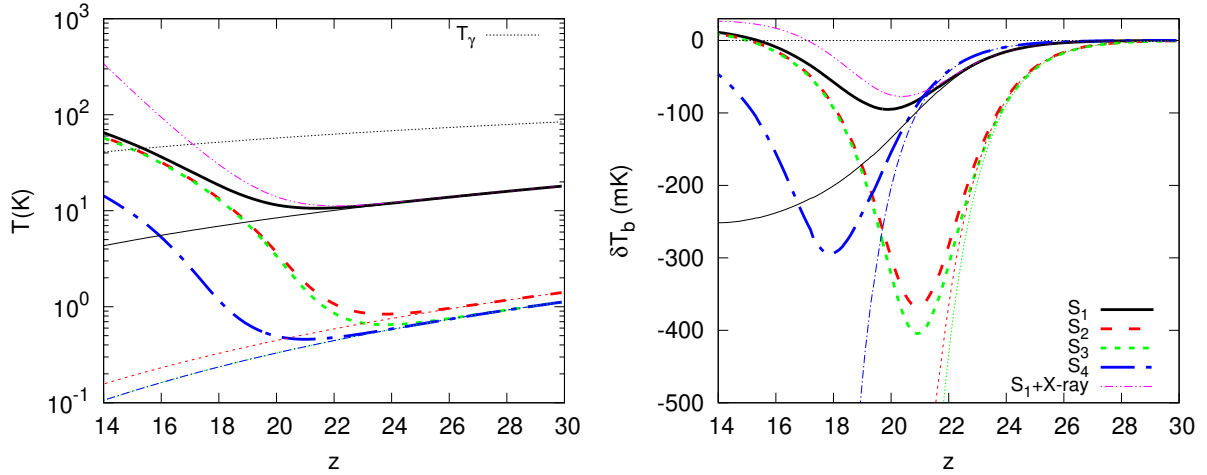


Figure 1. Left-hand panel: The redshift evolution of the gas temperature for the different scenarios described in Section 3.1. See Table 1 for the details of the scenarios. The thin lines show the cases without $\text{Ly}\alpha$ heating, the thick lines the cases with $\text{Ly}\alpha$ heating. The double dot-dashed curve shows the case of model S_1 with X-ray heating but without $\text{Ly}\alpha$ heating. The black dotted curve indicates the evolution of the CMB temperature with redshift. Right-hand panel: The redshift evolution of the volume averaged differential brightness temperature δT_b for the same scenarios.

et al. 1999). The results show that for our cosmological parameters the $T_K \propto (1+z)^2$ relation is valid below $z_0 \approx 138$. Expressed in the same form as the $\text{Ly}\alpha$ heating rate in Equation 8, this adiabatic or Hubble cooling is given as

$$\left. \frac{d \log T_K}{d \log t} \right|_H = -\frac{4}{3}.$$

However, as pointed out by Bowman et al. (2018) these cooling processes are unable to explain the strong absorption signal at redshift 17 found in the EDGES low-band results as it requires a lower temperature than can be achieved using standard cosmological models. In order to reproduce the EDGES results we therefore include an excess cooling rate in our calculations. As the origin of the excess cooling is not clear, we adopt a simple parametric model inspired by Mirocha & Furlanetto (2019). In this, the excess cooling rate is written as

$$\left. \frac{d \log T_K}{d \log t} \right|_{\text{cool}} = \alpha \left[\frac{1+z}{1+z_0} \right]^\beta, \quad (11)$$

where the parameters $\alpha \leq 0$ and β determine the strength and redshift dependence of the excess cooling rate respectively. We only apply this excess cooling rate for redshifts $z \leq z_0$.

3 RESULTS

To gain insight into the impact of $\text{Ly}\alpha$ heating on the volume averaged 21-cm signal from the CD, we first explore several individual scenarios. Later we will extend this study by exploring the parameter space of the excess cooling and average $\text{Ly}\alpha$ flux. We will also investigate scenarios that can explain the strong absorption signal as reported by the EDGES low-band observation.

3.1 Main scenarios

We will first consider four different choices for excess cooling so as to study the impact of different parameters/processes on the evolu-

Scenarios	f_α	α	β	$\delta T_{b,\text{min}}$	$z(\delta T_{b,\text{min}})$	Δz
S_1	1.0	0.0	0.0	-95.1	19.9	4.6
S_2	1.0	-1.0	0.0	-367.1	20.9	3.7
S_3	1.0	-1.0	-0.1	-404.6	20.9	3.6
S_4	0.1	-1.0	-0.1	-294.4	17.9	4.2

Table 1. The $\text{Ly}\alpha$ efficiency and excess cooling parameters for the four different scenarios considered in Sect. 3.1. Also shown are the quantities which describe the resulting absorption profile, $\delta T_{b,\text{min}}$, $z(\delta T_{b,\text{min}})$ and Δz which represent the minimum brightness temperature, its corresponding redshift and the FWHM of the absorption profiles, respectively.

Parameters	Min range	Max Range
f_α	0.01	100.0
α	-1.5	0.0
β	-0.5	0.5

Table 2. The range of the three parameters explored in this study.

tion of δT_b . The parameters for these scenarios are listed in Table 1. The fiducial model S_1 has $\alpha = 0$ and therefore does not include the additional cooling. The left-hand panel of Fig. 1 presents the redshift evolution of the average gas temperature of the neutral regions in the IGM for these four choices. For each, we consider two cases, namely without (thin lines) and with (thick lines) $\text{Ly}\alpha$ heating. For the choice of no excess cooling S_1 we also consider a case without $\text{Ly}\alpha$ heating but with heating by X-ray sources (thin double dot-dashed curve).

For the cases without $\text{Ly}\alpha$ and X-ray heating, the temperature keeps decreasing over time as no other heating mechanisms

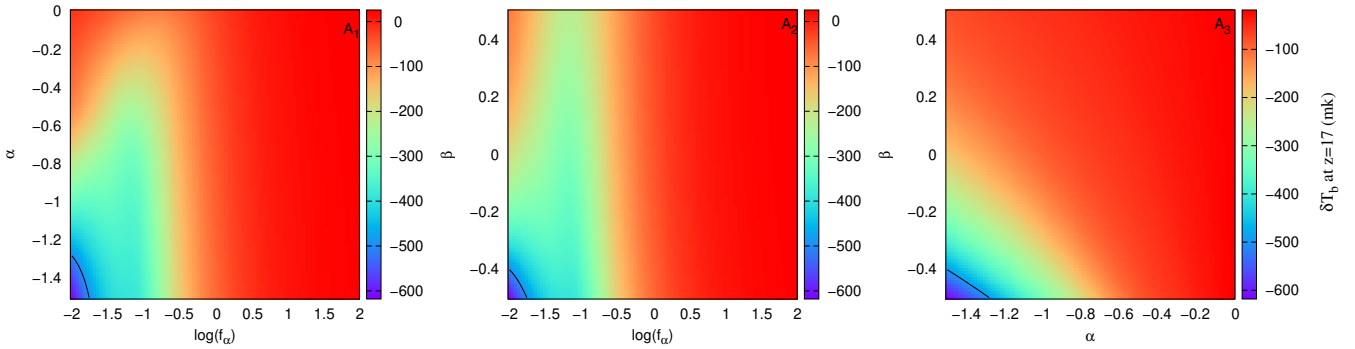


Figure 2. The different panels in the figure show the averaged brightness temperature at redshift 17 as a function of two different parameters at a time. All these 2D slices contain the minimum δT_b estimated from exploring the parameter ranges as stated in Table 2. While we vary two parameters at a time in these slices, the third parameter is fixed such that the slices correspond to the minimum brightness temperature at redshift 17 for the entire parameter space. In this case, the third parameter values are $\beta = -0.5$, $\alpha = -1.5$ and $f_\alpha = 0.01$ which correspond to panels A_1 , A_2 and A_3 respectively. The black contours represent -500 mK brightness temperature as reported by EDGES low-band observation. We fix $T_{\text{vir}} = 10^4$ K for these models.

are included in these scenarios. When we include Ly α heating, it impacts the gas temperatures as early as redshift 22 in all these scenarios. For the scenario without excess cooling, the gas temperature increases to ~ 60 K at redshift ~ 14 which is roughly consistent with the results of Chuzhoy & Shapiro (2007). The small difference is due to ignoring the contribution from deuterium in our calculations. When we instead of Ly α heating include X-ray heating according to the description in Sect. 2.1, the gas temperature for S_1 increases more rapidly and reaches ~ 300 K by $z \sim 14$. This is why Ly α heating is often ignored in simulations as X-ray heating will quickly dominate. However, if X-ray heating is inefficient or absent, Ly α heating will have a non-negligible impact on the IGM temperature.

As the other three choices S_2 – S_4 include excess cooling, the Cosmic Dawn starts at lower gas temperatures. In S_2 the excess cooling does not have a redshift dependence, in S_3 it increases with time. S_4 has the same excess cooling parameters as S_3 but a ten times lower Ly α efficiency. When including the heating due to the scattering of Ly α photons, it impacts the temperatures in S_2 and S_3 earlier compared to S_1 , although the background Ly α flux densities for these models are identical. This is due to the fact that the Ly α heating rates increases as the kinetic temperature decreases (see equation 8). As expected the heating starts later for a lower Ly α background (S_4).

S_1 , S_2 and S_3 all start with different temperatures. However, by ~ 16 they all reach almost the same equilibrium temperature due to Ly α heating. For $\alpha = 1$ the excess cooling can thus not compete with Ly α heating. For the case of a lower Ly α flux (S_4), the heating is delayed and remains weaker compared to the other scenarios.

The right-hand panel of Fig. 1 shows the redshift evolution of the global 21-cm signal corresponding to the nine scenarios (S_1 through S_4 with and without Ly α heating and S_1 with X-ray heating). When calculating δT_b we always include the Ly α coupling for the spin temperature, even in those models where we ignore Ly α heating. As for all these scenarios the IGM remains highly neutral at redshifts > 14 , the average brightness temperature is mostly determined by the gas temperature and the strength of this Ly α coupling. As the background Ly α flux is low at high redshift ($z \sim 30$), the coupling between T_S and T_K is weak and T_S re-

mains close to T_γ . This makes $\delta T_b \approx 0$ at those redshifts. As more sources form with time, Ly α coupling becomes stronger and the signal starts to appear in absorption, i.e., with a negative sign. However, different heating processes can increase the gas temperature and eventually δT_b transitions from absorption to emission. This produces a characteristic trough-like feature in the redshift evolution of δT_b , which we refer to as the ‘absorption profile’.

In the absence of Ly α heating, δT_b decreases with redshift as T_K decreases with time and the signal remains in absorption until reionization ends. In such cases, δT_b slowly decreases to ~ -250 mK at redshift ~ 15 for S_1 without excess cooling (thin solid line), while δT_b rapidly decreases to values below ~ -500 mK at redshift $\lesssim 20$ for models S_2 through S_4 which include excess cooling (thin long-dashed, short-dashed and dot-dashed lines).

In the presence of Ly α heating, the increase of gas temperature as early as redshift ~ 20 resists the decrease of δT_b with time and produces prominent absorption troughs (thick lines). The minimum δT_b values of these absorption profiles are much less deep than the corresponding signals from the no heating cases, demonstrating the large impact Ly α heating has. For example in model S_1 the absorption profile does not reach below -100 mK and for S_2 and S_3 not below -400 mK.

The absorption profiles can be described by the minimum value of the brightness temperature ($\delta T_{b,\text{min}}$), the corresponding redshift $z(\delta T_{b,\text{min}})$ and the full width at half maximum (FWHM) of the absorption profile (Δz). We list the values for the cases with Ly α heating in Table 1. These numbers clearly depend on the excess cooling rate and Ly α heating rates. We see the absorption profiles are much stronger and appear earlier for models S_2 and S_3 than for model S_1 . This is due to the excess cooling in the former models which results in a lower initial gas temperature compared to S_1 . The values for the FWHM Δz are lower when excess cooling is present.

When the Ly α background is lower ($f_\alpha = 0.1$, S_4) the absorption profile becomes less deep, wider and appears later compared to a model which has $f_\alpha = 1$ (S_3), even though the gas temperature is actually lower. However, the profile can still reach a minimum of ~ -300 mK, below what can be achieved without excess cooling.

For completeness, the right-hand panel of Fig. 1 also shows

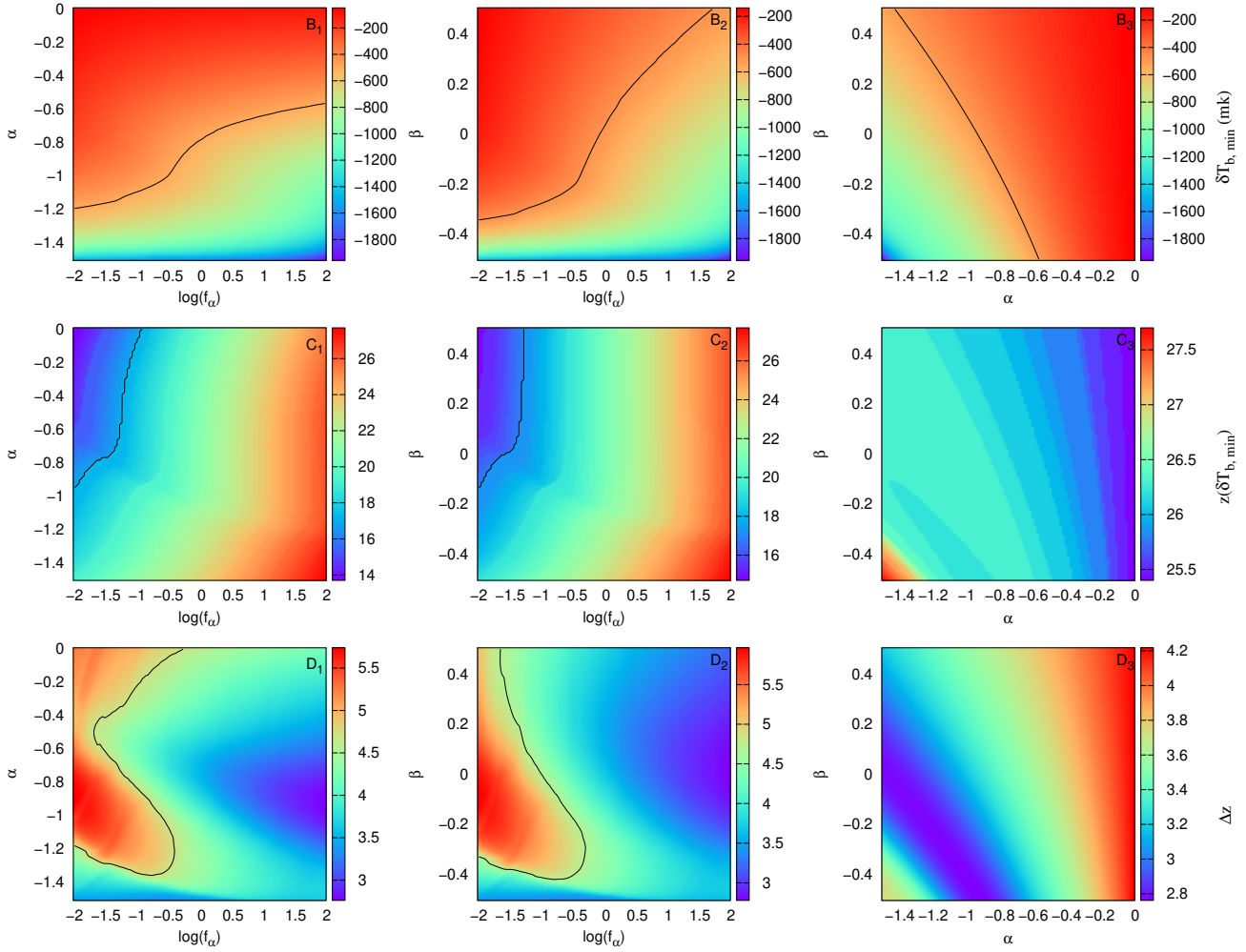


Figure 3. The upper panels represent the minimum brightness temperature throughout the reionization for the 2D slices of the parameter space. The third parameter is fixed such that the slices contain the minimum brightness temperature obtained while exploring the entire 3D parameter space. In this case, the third parameter values are $\beta = -0.5$, $\alpha = -1.5$ and $f_\alpha = 100$ which correspond to panels B_1 , B_2 and B_3 respectively. The middle row panels represent the associated redshifts to these minimum δT_b . We fix $T_{\text{vir}} = 10^4$ K for these models. The bottom panels show the FWHM of the absorption trough of these models. The contours from top to bottom panels of the figure represent $\delta T_{b,\text{min}} = -500$ mK, $z(\delta T_{b,\text{min}}) = 17.2$ and FWHM $\Delta z = 4.7$ respectively which characterize the absorption profile as reported by EDGES low-band observation.

the differential brightness temperature evolution for the model without excess cooling and $\text{Ly}\alpha$ heating but with X-ray heating (thin dot-dot-dashed curve). Due to the higher temperatures, this absorption profile is less deep and somewhat narrower than the corresponding case without X-ray heating but with $\text{Ly}\alpha$ heating (thick solid curve).

3.2 Parameter space study

Now we will explore the parameter space of excess cooling (α and β) and $\text{Ly}\alpha$ flux (f_α) to find the impact on the absorption signal from the CD in terms of $\delta T_{b,\text{min}}$, $z(\delta T_{b,\text{min}})$ and Δz . The details of the parameter space are given in Table 2. As the excess cooling is due to unknown processes, the parameter ranges for α and β chosen here are somewhat arbitrary. However, as we will see this range covers the most interesting results in terms of the absorption feature and the EDGES low-band results.

We will study the global 21-cm signal around redshift ~ 17 which corresponds to $z(\delta T_{b,\text{min}})$ of the EDGES low-band detection. The different panels of Figure 2 represent the value of the differential brightness temperature at redshift 17 in 2D slices through the 3D parameter space. For these slices, the third parameter is chosen such that these slices contain the minimum brightness temperature at $z = 17$ within the explored parameter space. The values are $\beta = -0.5$ (panel A_1), $\alpha = -1.5$ (panel A_2) and $f_\alpha = 0.01$ (panel A_3).

The resonance photons impact the signal in two ways: (i) heating due to resonance scattering decreases for a lower background $\text{Ly}\alpha$ flux, (ii) coupling of T_S with T_K decreases for a lower $\text{Ly}\alpha$ background. These two effects create the vertical feature in δT_b around $f_\alpha \sim 0.1$ in panels A_1 and A_2 . In the presence of significant $\text{Ly}\alpha$ heating (e.g. for $f_\alpha > 1$), the amplitude of δT_b at redshift 17 remains small for all values of α and β . As shown in panel A_3 , strong excess cooling ($\alpha \sim -1.5$ and $\beta \sim -0.5$) can produce a

deep absorption feature but only for a very weak Ly α flux, reaching values as low as -600 mK for $f_\alpha \sim 0.01$.

We note that the color bar associated with the panels of Fig. 2 represent δT_b at redshift 17, not $\delta T_{b,\min}$ for the choice of parameters. This figure shows that $\delta T_b \sim -500$ mK at redshift 17 is only possible for a weak Ly α background and strong excess cooling rates as shown by the contours in the panels. However, this does not mean that the values of δT_b in this figure are equal to $\delta T_{b,\min}$, the minimum of the absorption profiles. Thus, we can not directly compare these with the EDGES low-band observations. However, we can see that a large part of the parameter space corresponds to δT_b values larger than -500 mK and thus, should be excluded by the EDGES observation. We will present a detailed investigation of this below.

First, we will investigate the behaviour of absorption profiles over the parameter space. The top row of panels of Fig. 3 show 2D slices of $\delta T_{b,\min}$ through the entire parameter space. As in Fig. 2, the third parameter is chosen such that these slices contain the lowest value of $\delta T_{b,\min}$ obtained within the entire parameter space. In this case, the values for the third parameter are $\beta = -0.5$, $\alpha = -1.5$ and $f_\alpha = 100$ which correspond to the left, middle and right panels, respectively. The middle row of panels shows the associated redshift $z(\delta T_{b,\min})$ of the minimum of the absorption profiles and the bottom row the corresponding FWHM Δz .

Panels B₁ and B₂ show that $\delta T_{b,\min}$ decreases with increasing f_α as the coupling between T_S and T_K becomes stronger. However, this also implies that Ly α heating becomes efficient earlier and thus the minima of the absorption profiles appear at higher redshifts when increasing f_α (see panels C₁, C₂). As shown in panel B₃, $\delta T_{b,\min}$ decreases for lower values of α and β which corresponds to stronger excess cooling and also in this case $z(\delta T_{b,\min})$ shifts towards higher redshifts (panel C₃). The CD starts with a lower gas temperature for smaller values of α and β . As the Ly α heating rate increases for lower temperatures, Ly α heating become efficient earlier for a stronger excess cooling model. These results are consistent with our findings in Section 3.1.

The bottom row of Fig. 3 show the corresponding FWHM Δz . The dependence of Δz on the parameters is more complex compared to what we saw for $\delta T_{b,\min}$ and $z(\delta T_{b,\min})$. We have to keep in mind a few facts before understanding the features in the bottom panels of the figure. One is that all models reach their equilibrium temperature due to Ly α heating approximately at the same redshift for a fixed Ly α background (as we have seen in section 3.1). Secondly, the initial temperature (at $z = 30$) of these models decreases rapidly with stronger cooling parameters. The absorption profile becomes deeper and shifts towards higher redshift for a larger excess cooling rate. On the other hand, the Ly α heating starts earlier and δT_b of these profiles approaches zero at a similar redshift. These two facts make Δz decrease initially with the increase of excess cooling rate for a fixed f_α as shown in panel D₃. However, Δz starts increasing for $\alpha < -1$ and $\beta < 0$ as the initial temperature of these models becomes smaller and the minima of the absorption profiles shifts towards higher redshifts. On the other hand, Ly α heating becomes efficient earlier for a larger value of f_α which decrease Δz for a fixed excess cooling (see panels D₁ and D₂).

The black lines in Fig. 3 correspond to the absorption profile parameters estimated from the EDGES low-band observation. However, as these slices correspond to the minimum δT_b calculated by exploring the whole 3D parameter space, an interpretation of EDGES results from these contours is difficult. We will discuss

the parts of the parameter space that are consistent with the EDGES absorption profile in the following section.

3.3 Interpretation of EDGES low-band results

Bowman et al. (2018) have reported a measurement of an absorption profile of δT_b with $\delta T_{b,\min} = -500^{+200}_{-500}$ mK at $z(\delta T_{b,\min})$ corresponds to 78 ± 1 MHz with FWHM Δz corresponding to 19^{+4}_{-2} MHz using observations with the EDGES low-band antenna. We will investigate what part of our parameter space agrees with this observation. However, we do not consider the detailed shape of the absorption profile as reported in Bowman et al. (2018), nor use parameter estimation techniques such as Markov chain Monte Carlo. Instead, we consider the values of $\delta T_{b,\min}$, $z(\delta T_{b,\min})$ and FWHM Δz corresponding to the profile to compare with the absorption profiles produced by our model. We would like to remind the reader that we have not included any X-ray heating in this parameter space study.

Here, we focus on models from the parameter space study which have profile parameters $\delta T_{b,\min}$, $z(\delta T_{b,\min})$ and FWHM Δz in agreement with the EDGES profile parameters within the 1σ errors quoted above. Figure 4 presents which values for our parameters agree with the EDGES low band results. The left-hand panel shows a 2D plot for parameters α and β where the colour of each point represents the average value of f_α for which the values of α , β are consistent with the EDGES observation. We see that two specific ranges of cooling parameters produce the desired profile, the broader of the two bands for a weak Ly α background flux ($f_\alpha < 0.08$) and the narrower one for a very weak Ly α background ($f_\alpha < 0.01$). The broader band is characterized by a strong but not too strong cooling around the redshift of the absorption profile ($-2 \lesssim (d \log T_K / d \log t)_{\text{cool}} \lesssim -1.2$) and the narrower band by a stronger value of $(d \log T_K / d \log t)_{\text{cool}} \sim -2.5$. This can also be characterized through the temperature which the IGM would achieve in the absence of Ly α heating. For the cooling parameters in the broader of the two bands, this temperature is between 0.2 and 0.3 K and between 0.05 and 0.06 K for the narrower band. For stronger cooling than shown in the left-hand panel, $\delta T_{b,\min}$ will be lower and will shift towards higher redshifts. Similarly, $z(\delta T_{b,\min})$ will shift towards higher redshifts for larger values of f_α .

The right-hand panel of Fig. 4 shows a 3D representation of our parameter space where the colour indicates the χ^2 value. We define χ^2 error in this plot as

$$\chi^2 = \sum_{i=1,3} \left(\frac{M_i - O_i}{\sigma_i} \right)^2, \quad (12)$$

where i represents there parameters to define the absorption profile used in this study, M and O are the model and observation parameters respectively and σ_i represents the 1σ error on the measured parameters considered here. One can notice that for a certain choice of cooling parameters a range of f_α values can satisfy the agreement condition. However, all f_α values are low. The isolated region $f_\alpha = 0.01$ corresponds to deeper absorption profiles with $\delta T_{b,\min} \lesssim -500$ mK while the other region has absorption depths $\delta T_{b,\min} \sim -300$ mK.

One thing to keep in mind that we have ignored all other heating processes such as X-ray heating, etc. If any other additional energy is added to the IGM, the excess cooling would have to compensate for this in order for the absorption profile to remain consistent with the EDGES result. In other words, the cooling rates derived here should be considered as lower limits. For example, the

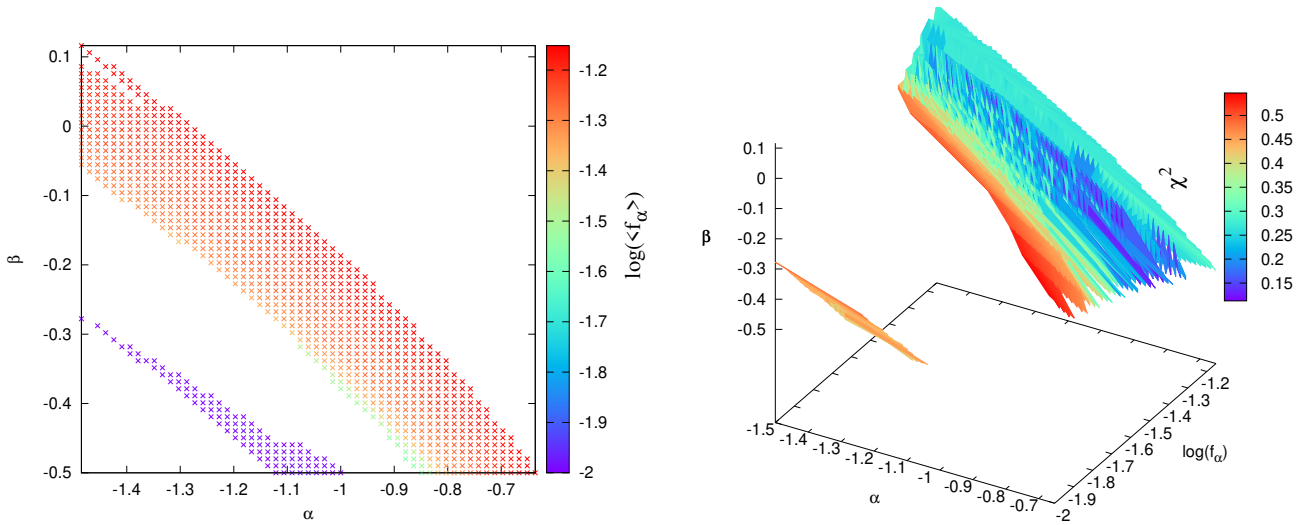


Figure 4. Left-panel: The crosses indicate the values of the excess cooling parameters α and β which produce absorption profiles that agree with the EDGES low band results within a 1σ error. The colour bar represents the average values of f_α for these matching models. Right panel: 3D plot of the parameter space which agrees with the EDGES low band results. The colour bar shows the χ^2 error as defined in equation 12.

combination $f_\alpha \lesssim 0.1$, $\alpha \sim -1.5$ and $\beta \sim 0.1$ corresponds to the minimum excess cooling required to achieve the strong signal reported by EDGES. This minimum excess cooling rate is already similar to the Hubble cooling rate at redshift 17.

4 CONCLUSIONS

In this study, we consider the heating contribution from resonance scattering of Ly α photons in the IGM during the Cosmic Dawn. This heating is an inevitable effect of the resonance scattering which also couples the spin temperature to the gas temperature. As we want to be able to reproduce the anomalously strong absorption signal reported from the EDGES low band observations, we consider an additional cooling rate besides the adiabatic Hubble cooling. The physical process responsible for such excess cooling remains uncertain but an interaction between baryons and dark matter particles is one possible cause.

Using this scenario, we investigate the evolution of the average differential brightness temperature of the 21-cm signal. We explore a three-dimensional parameter space defined by two parameters describing the excess cooling (α and β) and one parameter setting the strength of the Ly α background (f_α) to study this global 21-cm signal from the CD. The main findings of the paper are listed below.

Without excess cooling, Ly α heating can start heating up the IGM as early as redshift 22 for a typical emissivity of ~ 10000 photons per baryon between Ly α and the Lyman limit. Although this heating rate is smaller than the usually assumed X-ray heating rates, still it can increase the gas temperature to several tens of K which is the equilibrium temperature between the heating by the continuum photons and cooling by the injected photons. This is consistent with previous studies such as Chuzhoy & Shapiro (2007). For this case, we find an absorption signal of depth ~ -100 mK at redshift ~ 20 .

When including excess cooling, the Cosmic Dawn starts with

a very cold IGM. In such cases, Ly α heating becomes efficient earlier and rapidly increases the IGM temperature to the equilibrium temperature. For these cases, we find absorption signals which are factors 3 – 4 deeper than without excess cooling.

When exploring the parameter space of the excess cooling rate and Ly α background, we find that the EDGES low-band results can only be reproduced for strong excess cooling combined with a weak Ly α background. This puts an upper bound on the background Ly α flux which is ~ 15 times lower than our fiducial choice. Thus the sources at redshift ~ 17 emit fewer Ly α photons or the star formation efficiency is lower than expected. This result disagrees with the findings of Mirocha & Furlanetto (2019) who claim that the star formation efficiency should be higher than expected in order to produce the strong Ly α background needed to achieve strong coupling between the spin and gas temperatures. However, these authors did not consider the effect of Ly α heating. In our exploration of parameter space, we frequently found interesting models at the edge of the parameter ranges that we considered. We did not explore a larger range of values as the trends still remain quite clear: only fairly strong cooling which without Ly α heating would give gas temperatures below ~ 0.3 K around $z \approx 17$ combined with a weak Ly α background ($f_\alpha \lesssim 0.06$) can reproduce the EDGES low-band results. Possibly even stronger cooling with an even weaker Ly α background would also give consistent results but such models become increasingly unlikely.

We did not explore the impact of changing the source population. In our models, all halos with a virial temperature above 10^4 K contribute to the Ly α background. Obviously increasing this limit would also reduce the background and possibly lead to models in which fiducial values for f_α combined with strong excess cooling could reproduce the EDGES low-band absorption profile. Lowering the minimum virial mass would only increase the Ly α background and thus require even lower values for f_α .

We did also not explore the impact of the star formation efficiency parameter f_* . However, for the redshift regime which we explore this parameter is degenerate with f_α .

We thus find that heating due to resonance scattering with Lyman series photons may have a significant impact during the Cosmic Dawn and thus should be taken into account when modelling the 21-cm signal. Although we do find that for a fiducial value of X-ray heating ($f_X = 1$), the Ly α heating is subdominant, many authors explore a wide range of values for f_X including low values for which Ly α heating will dominate over X-ray heating (e.g. [Cohen et al. 2017](#); [Greig & Mesinger 2018](#); [Monsalve et al. 2019](#)). We note that none of these papers actually include the effect of Ly α heating. Models to explain the absorption feature seen in the EDGES results rely on Ly α coupling to produce an observable signal and thus any excess cooling needs to overcome the heating caused by this coupling. It remains to be seen if processes such as cooling of baryons through interactions with dark matter particles can achieve this.

ACKNOWLEDGEMENTS

The authors would like to thank Anastasia Fialkov, Sambit Giri, Tirthankar Roy Choudhury for useful discussions regarding this work. We have also used resources provided by the Swedish National Infrastructure for Computing (SNIC) (proposal number SNIC 2018/3-40) at PDC, Royal Institute of Technology, Stockholm.

REFERENCES

- Barkana R., 2018, *Nature*, **555**, 71
- Barkana R., Outmezguine N. J., Redigolo D., Volansky T., 2018, arXiv e-prints, p. [arXiv:1803.03091](#)
- Berlin A., Hooper D., Krnjaic G., McDermott S. D., 2018, *Phys. Rev. Lett.*, **121**, 011102
- Bowman J. D., Rogers A. E. E., 2010, *Nature*, **468**, 796
- Bowman J. D., et al., 2013, *Publ. Astron. Soc. Australia*, **30**, e031
- Bowman J. D., Rogers A. E. E., Monsalve R. A., Mozdzen T. J., Mahesh N., 2018, *Nature*, **555**, 67
- Chen X., Miralda-Escudé J., 2004, *ApJ*, **602**, 1
- Chuzhoy L., Shapiro P. R., 2007, *ApJ*, **655**, 843
- Clark S. J., Dutta B., Gao Y., Ma Y.-Z., Strigari L. E., 2018, *Phys. Rev. D*, **98**, 043006
- Cohen A., Fialkov A., Barkana R., Lotem M., 2017, *MNRAS*, **472**, 1915
- Cohen A., Fialkov A., Barkana R., 2018, *MNRAS*, **478**, 2193
- D’Amico G., Panci P., Strumia A., 2018, *Phys. Rev. Lett.*, **121**, 011103
- Ewall-Wice A., Chang T.-C., Lazio J., Doré O., Seiffert M., Monsalve R. A., 2018, *ApJ*, **868**, 63
- Feng C., Holder G., 2018, *ApJ*, **858**, L17
- Fialkov A., Barkana R., 2019, arXiv e-prints, p. [arXiv:1902.02438](#)
- Fialkov A., Cohen A., Barkana R., Silk J., 2017, *MNRAS*, **464**, 3498
- Fialkov A., Barkana R., Cohen A., 2018, *Physical Review Letters*, **121**, 011101
- Field G. B., 1958, *Proceedings of the IRE*, **46**, 240
- Fraser S., et al., 2018, *Physics Letters B*, **785**, 159
- Furlanetto S. R., Loeb A., 2004, *ApJ*, **611**, 642
- Furlanetto S. R., Pritchard J. R., 2006, *MNRAS*, **372**, 1093
- Ghara R., Choudhury T. R., Datta K. K., 2015, *MNRAS*, **447**, 1806
- Ghara R., Choudhury T. R., Datta K. K., Choudhuri S., 2016, *MNRAS*, **453**, 1806
- Ghosh A., Prasad J., Bharadwaj S., Ali S. S., Chengalur J. N., 2012, *MNRAS*, **426**, 3295
- Greenhill L. J., Bernardi G., 2012, preprint, ([arXiv:1201.1700](#))
- Greig B., Mesinger A., 2018, *MNRAS*, **477**, 3217
- Hirata C. M., 2006, *MNRAS*, **367**, 259
- Liu H., Slatyer T. R., 2018a, arXiv e-prints, p. [arXiv:1803.09739](#)
- Liu H., Slatyer T. R., 2018b, *Phys. Rev. D*, **98**, 023501
- Madau P., Meiksin A., Rees M. J., 1997, *ApJ*, **475**, 429
- McQuinn M., Furlanetto S. R., Hernquist L., Zahn O., Zaldarriaga M., 2005, *ApJ*, **630**, 643
- Mellema G., Koopmans L., Shukla H., Datta K. K., Mesinger A., Majumdar S., 2015, *Advancing Astrophysics with the Square Kilometre Array (AASKA14)*, p. 10
- Mesinger A., Ferrara A., Spiegel D. S., 2013, *MNRAS*, **431**, 621
- Mirocha J., Furlanetto S. R., 2019, *MNRAS*, **483**, 1980
- Mitridate A., Podo A., 2018, *Journal of Cosmology and Astro-Particle Physics*, **2018**, 069
- Monsalve R. A., Fialkov A., Bowman J. D., Rogers A. E. E., Mozdzen T. J., Cohen A., Barkana R., Mahesh N., 2019, arXiv e-prints, p. [arXiv:1901.10943](#)
- Muñoz J. B., Loeb A., 2018, arXiv e-prints, p. [arXiv:1802.10094](#)
- Nebrin O., Ghara R., Mellema G., 2018, arXiv e-prints, p. [arXiv:1802.10094](#)
- Paciga G., et al., 2013, *MNRAS*, **433**, 639
- Park J., Mesinger A., Greig B., Gillet N., 2019, *MNRAS*, **484**, 933
- Parsons A. R., et al., 2014, *ApJ*, **788**, 106
- Patil A. H., et al., 2017, *ApJ*, **838**, 65
- Patra N., Subrahmanyam R., Sethi S., Udaya Shankar N., Raghunathan A., 2015, *ApJ*, **801**, 138
- Planck Collaboration et al., 2016, *A&A*, **594**, A13
- Pritchard J. R., Furlanetto S. R., 2007, *MNRAS*, **376**, 1680
- Ross H. E., Dixon K. L., Ghara R., Iliev I. T., Mellema G., 2018, preprint, ([arXiv:1808.03287](#))
- Santos M. G., Amblard A., Pritchard J., Trac H., Cen R., Cooray A., 2008, *ApJ*, **689**, 1
- Schneider A., 2018, *Phys. Rev. D*, **98**, 063021
- Seager S., Sasselov D. D., Scott D., 1999, *ApJ*, **523**, L1
- Sharma P., 2018, *MNRAS*, **481**, L6
- Sokolowski M., et al., 2015, *Publ. Astron. Soc. Australia*, **32**, e004
- Tingay S. J., et al., 2013, *Publications of the Astronomical Society of Australia (PASA)*, **30**, 7
- Venumadhav T., Dai L., Kurov A., Zaldarriaga M., 2018, *Phys. Rev. D*, **98**, 103513
- Voytek T. C., Natarajan A., Jáuregui García J. M., Peterson J. B., López-Cruz O., 2014, *ApJ*, **782**, L9
- Wouthuysen S. A., 1952, *AJ*, **57**, 31
- van Haarlem M. P., et al., 2013, *A&A*, **556**, A2

This paper has been typeset from a $\text{\TeX}/\text{\LaTeX}$ file prepared by the author.